International Journal of Biological Macromolecules 205 (2022) 220–230

Contents lists available at ScienceDirect

International Journal of Biological Macromolecules

journal homepage: www.elsevier.com/locate/ijbiomac

Critical comparison of the properties of cellulose nanofibers produced from softwood and hardwood through enzymatic, chemical and mechanical processes

Jose Luis Sanchez-Salvador [a], Cristina Campano [a,b], Ana Balea [a], Quim Tarrés [c], Marc Delgado-Aguilar [c], Pere Mutjé [c], Angeles Blanco [a], Carlos Negro [a,*]

[a] Department of Chemical Engineering and Materials, Universidad Complutense de Madrid, Avda. Complutense s/n, 28040 Madrid, Spain
[b] Department of Microbial and Plant Biotechnology, Centro de Investigaciones Biológicas Margarita Salas (CIB-CSIC), 28040 Madrid, Spain
[c] Group LEPAMAP, Department of Chemical Engineering, University of Girona, C/M. Aurèlia Campmany 61, 17071 Girona, Spain

ARTICLE INFO

Keywords:
Nanocellulose
Cellulose nanofibers
TEMPO-mediated oxidation
Enzymatic pretreatment
Refining
Gel point
Microscopy
Rheology
Softwood
Hardwood

ABSTRACT

Current knowledge on the properties of different types of cellulose nanofibers (CNFs) is fragmented. Properties variation is very extensive, depending on raw materials, effectiveness of the treatments to extract the cellulose fraction from the lignocellulosic biomass, pretreatments to facilitate cellulose fibrillation and final mechanical process to separate the microfibrils. Literature offers multiple parameters to characterize the CNFs prepared by different routes. However, there is a lack of an extensive guide to compare the CNFs. In this study, we perform a critical comparison of rheological, compositional, and morphological features of CNFs, produced from the most representative types of woody plants, hardwood and softwood, using different types and intensities of pretreatments, including enzymatic, chemical and mechanical ones, and varying the severity of mechanical treatment focusing on the relationship between macroscopic and microscopic parameters. This structured information will be exceedingly useful to select the most appropriate CNF for a certain application based on the most relevant parameters in each case.

1. Introduction

Cellulose has been physically and chemically modified to produce a broad spectrum of materials and nanomaterials, where cellulose nanofibers (CNFs) are one of the main products [1,2]. CNFs are fibrillated nanoparticles, obtained mainly through the application of mechanical treatments to lignocellulose [3]. This process causes the delamination of cellulose, obtaining micro or nanofibers with amorphous and crystalline regions of high aspect ratio [4,5]. The most common mechanical processes used in the fibrillation of cellulose are high-pressure homogenization (HPH), microfluidization, grinding, refining or cryocrushing [6], among others. These treatments require high energy to break down the fibers structure and, on some occasions, the final product is still far from being homogeneously downscaled [7,8].

For these reasons, the use of chemical, mechanical or enzymatic pretreatments, is essential [9]. Among them, chemical oxidation, via carboxylation using 2,2,6,6-tetramethylpiperidine-1-oxyl (TEMPO) and NaBr as catalysts, and NaClO as oxidant, is one of the most used processes to obtain a homogenized sample with mostly individual fibrils, high aspect ratio, and diameters below 10 nm [10,11]. However, this reaction presents some drawbacks related to the high cost of TEMPO catalyst, or its recovery at the end of the process, which would help to increase its profitability and reduce the environmental impact due to the alkaline waste streams associated with the reaction medium that has a high amount of salts [12,13].

On the other hand, although high fibrillation and homogeneity are needed in some applications such as the obtention of nanopapers and nanofilms [14,15] or in biomedical and pharmaceutical applications [16]; other applications do not always require highly fibrillated and homogeneous CNFs, such as cement [17,18], paper or cardboard [19] reinforcement. In these occasions, it is possible to use soft pretreatments that produce cellulose microfibers (CMFs) such as enzymatic hydrolysis or mechanical refining, reducing the environmental impact and costs of CNF preparation [19,20].

With all that, the opportunities to obtain different types of CNFs are very wide, even more if we consider the variety of raw materials

* Corresponding author.
E-mail address: cnegro@ucm.es (C. Negro).

https://doi.org/10.1016/j.ijbiomac.2022.02.074
Received 31 December 2021; Received in revised form 1 February 2022; Accepted 13 February 2022
Available online 17 February 2022

available for their production, mainly from wood but also from other plants, algae, bacteria or tunicates [21]. The most studied group, the woody plants, is classified into hardwood and softwood species. Some differences between these types of species are the hemicellulose and lignin content. While the most common hemicellulosic monomer in hardwood is xylose, mannose is predominant in softwood [22,23]. In the case of lignin, softwood is composed mainly by guaiacyl units, whereas hardwood lignin has both syringyl and guaiacyl units with a more complex and heterogeneous structure [22,24]. This composition makes softwood pulp easier to fibrillate than hardwood pulp, which typically requires a more intensive process [24].

Literature from the last decade shows some studies that relate the differences in CNF preparation from different raw materials, comparing some characterization parameters [22,25,26], others compare chemical, enzymatic and mechanical pretreatments, but mainly focused on specific applications [19,20,22,27] or only relating few pretreatment conditions [28–31]. However, to the best of our knowledge, there are no studies providing a deep comparison between CNFs produced from the most representative types of woody plants, hardwood and softwood, using different types of pretreatments and intensities and also the variation in the severity of mechanical treatments, including rheological, morphological, chemical and compositional changes.

In this work, two common cellulose sources are used to produce CNFs: pine and eucalyptus, which were previously bleached and treated by Kraft process. 50 types of CNFs were prepared using three pretreatments: enzymatic, refining as mechanical pretreatment, and TEMPO-mediated oxidation as chemical pretreatment. After then, the intensity of HPH was tested at 5 pressure sequences. The characterization of CNF samples is critically discussed comparing the differences between the raw materials, pretreatments and homogenization severity using several quantitative parameters. A direct relationship between rheological and morphological properties has been found. Two techniques recently developed by these research groups are used in this study to describe fibers morphology: the skeleton analysis of CNF microscopy images to obtain the slope between the number of nodes of the fibers and their projected area [26] and the determination of the 2D fractal dimension (Df) [32].

2. Materials and methods

2.1. Materials

Bleached kraft softwood pulp from pine (BKSP) was kindly provided by Arauco (Chile) and bleached kraft hardwood pulp from eucalyptus (BKHP) was supplied from ENCE (Navia, Spain). The reagents used for TEMPO-mediated oxidation were 10% w/v NaClO, TEMPO reagent and NaBr (Merck, Spain), whereas for enzymatic pretreatment a solution of Novozym 476 with 2% of cellulases and activity factor of 4500 CNF-Ca/g cellulose (tested over a CMC substrate) was supplied by Novozymes A/S (Kalundborg, Denmark). Other reagents used were NaOH, HCl, NaCl or H_2SO_4 supplied by (Merck, Spain), crystal violet (Sigma) and Poly-L-Lysine solution, obtained from Electron Microscopy Sciences.

2.2. Pretreatments of cellulose

BKSP and BKHP were disintegrated by using a pulp disintegrator (PTI, Vorchdorf, Austria) at 90,000 revolutions and 1.5 wt% consistency after being soaked in water for one day to favor the swelling of fibers.

Three types of pretreatments were used previous the main mechanical treatment: mechanical pretreatment was carried out in a PFI mill for 20,000 revolutions (Hamjem Maskin AS, Hamar, Norway) to refine the disintegrated pulp sample, previously adjusted to 10 wt%. Enzymatic hydrolysis was conducted in a stirred pulp suspension with a consistency of 5 wt%, pH 4.8, and 50 °C. The enzyme solution Novozym 476 was dropped into the suspension at 80 (H80) and 240 mg/g of pulp (H240). The reaction was maintained for 4 h under stirring conditions. The hydrolysis was finished by increasing the temperature up to 80 °C for 30 min. Then, the enzymatically hydrolyzed pulp was washed with distilled water and kept at 4 °C. The third pretreatment was the chemical, using TEMPO-mediated oxidation performed like the methodology accounted by Saito et al. [33]. In this case, two oxidation levels, 5 (T5) and 15 mmol NaClO/g pulp (T15), were tested. It was considered that the reaction was over when pH remained constant without further NaOH addition.

2.3. Production of cellulose nanofibers

After pretreatments, pulps were adjusted to 1 wt% consistency and then, fibrillated to produce CNFs by high-pressure homogenization (HPH) in a laboratory homogenizer NS1001L PANDA 2K-GEA (GEA Niro Soavy, Parma, Italy). To achieve different nanofibrillation yields, five progressive pressure sequences were carried out:

- HPH1: 3 passes at 300 bars.
- HPH2: 3 passes at 300 bars + 1 passes at 600 bars.
- HPH3: 3 passes at 300 bars + 3 passes at 600 bars.
- HPH4: 3 passes at 300 bars + 3 passes at 600 bars + 1 passes at 900 bars.
- HPH5: 3 passes at 300 bars + 3 passes at 600 bars + 3 passes at 900 bars.

2.4. Compositional characterization

Cellulose, hemicellulose, extractives, ash, Klason and soluble lignin were measured in both the initial raw materials and the pretreated samples. Extractive contents were quantified from Soxhlet extraction according to TAPPI T204. Total lignin, cellulose, and hemicellulose contents were obtained following NREL/TP-510-42618 standard. Cellulose sample (300 mg) was hydrolyzed with 3 mL of 72 wt% H_2SO_4 for 1 h at 30 °C. Then, deionized water (84 g) was added to the sample which was introduced in an autoclave for 1 h at 121 °C. Hydrolyzed samples were vacuum filtered and the Klason lignin was determined from the sediment that remained in the filter. From this filter, ash content was determined by calcination at 525 °C according to TAPPI T211. On the other hand, the soluble lignin was obtained by measuring the absorbance of the filtrate in the UV–Visible spectrophotometer. The amount of hemicellulose and cellulose were analyzed by HPLC from the filtrate after neutralization with $CaCO_3$ and filtered through 0.2 μm filters.

2.5. Structural and chemical characterization

Crystallinity index (CrI) of raw materials was obtained by X-ray diffraction (XRD) with a Philips X'Pert MPD X-Ray diffractometer with an auto-divergent slit fitted with a graphite monocromator using Cu-Kα radiation according to Campano et al. (2018) [34]. Then, Segal's method was used to determine CrI [35]. The crystalline length was determined as the length of the nanocrystalline particles (CNC) extracted after submitting cellulose to acid hydrolysis with 64% H_2SO_4 at 45 °C for 45 min, following the procedure described by Campano et al. [36]. Transmission Electron Microscopy (TEM) images were taken and, at least, 30 individual particles were directly measured using the Image J software.

Finally, carboxyl content and cationic demand (CD) were determined by conductometric titration and colloidal titration, respectively, according to Delgado-Aguilar et al. (2015) [37].

2.6. Morphological characterization

2.6.1. Macroscopic analysis

Aspect ratio was obtained by a simplification of the gel point (GP) methodology based on the sedimentation of the fibers at low consistency [38]. Briefly, GP is simplified by replacing the derivative at the origin of

the curve initial concentration (C_o) vs. the sediment height (Hs/Ho) by the quotient between C_o and Hs/Ho (Eq. (1)). Optimal C_o was selected to obtain a Hs/Ho around 4–12%. Lower sedimentations produce difficulties to measure the height accurately, whereas a higher sedimentation deposit would cause a wide error in the substitution of the derivative by an increment. That is why, on some occasions, second sedimentation must be carried out with other C_o closer to the optimal one [38].

$$GP = \lim_{H_s/H_o \to 0} \left(\frac{dC_o}{d\left(H_s/H_o\right)} \right) \approx \frac{C_o(i)}{\left(Hs/Ho\,(i)\right)} \quad (1)$$

To prepare the samples, CNF suspensions were diluted using deionized water and stirred for 10 min. Then, 200 μL of crystal violet 0.1 wt% were added during the agitation to favor the sediment visualization [39]. 250 mL of the suspensions were left to settle into graduated cylinders until reach a steady value that indicated the complete deposition of fibers.

Aspect ratio was calculated from the GP according to Varanasi et al. (2013) [40], assuming a density of fibers around 1500 kg/m^3 and using the crowding number theory (Eq. (2)) [41].

$$Aspect\ ratio = 5.9 \cdot \left(\frac{\mathrm{GP}\left(\frac{\mathrm{kg}}{\mathrm{m3}}\right)}{1000} \right)^{-0.5} \quad (2)$$

Other macroscopic parameters calculated are transmittance and nanofibrillation yield [42,43]. Transmittance of CNF suspensions was determined using a UV–Vis Shimadzu spectrophotometer UV-160A using distilled water as reference and background. Nanofibrillation yield was calculated after centrifugation of each CNF sample (0.1 wt%) at 4500 rpm for 20 min. The nanofibrillated fraction remains in the supernatant while the non-fibrillated fraction is retained in the sediment. An aliquot of the supernatant was recovered, weighed, and dried in the oven until constant weight. Then, the yield was calculated as Eq. (3).

$$Nanofibrillation\ Yield\ (\%) = \frac{Dry\ weight\ of\ supernatant}{Dry\ weight\ of\ centrifuged\ sample} \cdot 100 \quad (3)$$

2.6.2. Microscopic analysis

CNFs were morphologically characterized by Optical Microscopy (OM) using a Zeiss Axio Lab.A1 optical microscope and a camera AxioCam ERc 5s under 5× magnification (Carl Zeiss Microscopy GmbH, Göttingen, Germany) and by TEM, carried out at the National Centre of Electronic Microscopy (Madrid, Spain) with a JEM 1400 microscope (JEOL, Tokio, Japan). To prepare the samples, 15 μL of 10% Poly-L-Lysine solution were added on a copper grid covered with a Formvar/carbon continuous layer. Then, 12 μL of 0.005 wt% CNF suspensions were deposited and left to dry before analysis [36]. OM and TEM micrographs were processed and analyzed to retrieve morphological information. In view of the large number of images, processing and analysis were automatized using various software scripts that have been reported in previous studies [26,44].

To measure branching index, images were first binarized using ImageJ, an open-source image processing software package. Images were segmented and the particles detected analyzed in terms of size and shape, and skeletonized according to the procedure described in a previous publication [45]. The number of nodes and branches were determined for each image skeleton obtained. The slope obtained from the linear regression of the curve number of nodes vs. projected area was used as branching degree.

On the other hand, the projected fractal dimension was measured on the micrographs. The acquired images were processed and analyzed using the same software. Images were firstly edited to achieve a good definition and high contrast of CNF borders. They were first converted into 8-bit images and then submitted to a bandpass filter and background subtraction to reduce the effect of impurities and irregularities in the images. Then, they were binarized through an auto threshold and corrected with a Close filter [44]. The fractal analysis was performed with the Fractal Box Count plugin.

2.7. Rheology

The viscous behavior of CNF suspensions is usually well-represented by the Herschel–Bulkley equation (Eq. (4)) [46,47]. Alternatively, yield stress (τ_o) is omitted from Eq. (4), using the apparent viscosity (η) as a function of the shear rate (γ) obtaining the Ostwald model as in Eq. (5):

$$\tau = \tau_o + K \cdot \gamma^n \quad (4)$$

$$\eta = K \cdot \gamma^{n-1} \quad (5)$$

where τ is shear stress, K is consistency index, and n the flow index. To measure the viscous behavior of the CNFs a Couette-type rheometer PCE-RVI 2 V1L rotational viscosimeter from PCE Instruments (Meschede, Germany) was used, equipped with the L3 spindle that rotates from 0.3–200 rpm, varying progressively γ and recording η. Conditions related to spindle shape and vessel were considered using a ratio between the diameter of the vessel and the spindle of 1.2 [48]. CNFs at 1 wt% consistency were tested five times with each material reporting an average of these five test runs.

3. Results

3.1. Characterization of raw and pretreated materials

Chemical composition and properties of raw materials have been shown to have a high impact on the type of fibrillation and on both microscopic and macroscopic properties of CNFs [24,49]. Fig. 1 shows the results from the compositional analysis performed to the raw materials. Both raw materials have been delignified using the same procedure but differences between both types of woods have triggered that cellulose extraction is not performed in the same way [50]. As it is already acknowledged, the amorphous regions of cellulose have a higher reactivity due to the disorder of the polymer chains [51]. This higher reactivity also applies to hydrogen bonding, that take place inherently either with water (swelling), between cellulose fibrils or with other polysaccharides, such as hemicelluloses [52]. As shown in Table 1, BKSP has a higher crystallinity index than BKHP, 78.3% compared to 72.7%. In addition, it has a higher crystalline length, which has been defined as the length of the crystalline regions isolated after acid hydrolysis, i.e. CNC. Thus, it is expected that the BKSP has a higher purity in terms of cellulose than BKHP, and it is indeed what is observed in Fig. 1. Apart from cellulose, the main difference between both raw materials relies on the percentage of hemicellulose that is still bonded with the cellulose fibers, which vary from 7.4% in the case of BKSP to 17.5% in the BKHP sample. These findings agree with previous studies [53–55].

Moreover, a slight variation was also observed in the content of lignin that is soluble in acid. Despite Klason or insoluble lignin is mostly removed during the pulp preparation process, a slight portion of lignin that is soluble in acid remains within the sample. Acid-insoluble lignin is considered to be of high molecular weight, while acid-soluble lignin presents a much lower molecular weight [56]. Considering, thus, the already mentioned higher content in amorphous cellulose of BKHP, it is reasonable that a higher proportion of low molecular weight lignin could have remained still attached to the fibers. Hence, the main conclusion that emerged from the compositional analysis of raw materials is that the higher proportion of amorphous cellulose present in BKHP limited the purification of cellulose in the kraft process.

Although aspect ratio refers to the length-width relationship of the

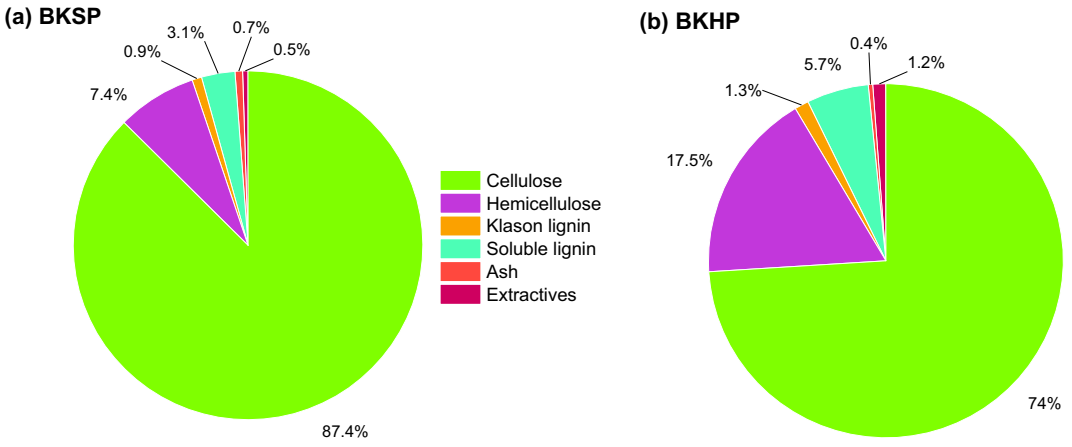

Fig. 1. Compositional analysis of pine (BKSP) and eucalyptus (BKHP) pulps.

Table 1
Morphological characterization of raw materials.

	BKSP	BKHP
Crystallinity index (%)	78.3	72.7
Crystalline length	189 ± 42	122 ± 56
Aspect ratio	75	59
Branching index (μm^{-2})	$3.65 \cdot 10^{-4}$	$2.43 \cdot 10^{-4}$
Df	1.660	1.426
Morphology (OM images)	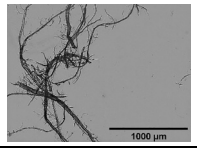	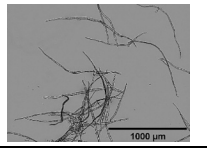

individual fibers, this parameter, in this study, could provide additional information on the behavior of the fibers in suspension, since it has been determined through the macroscopic behavior of samples during sedimentation [57]. In this case, BKSP exhibited a higher value than BKHP, and it agreed with the size of the fibers observed in OM (Table 1). However, this value could have been affected by the different swelling behavior of both raw materials, which is directly related to the charge of the fibers [52]. Since BKHP has a higher swelling ability, the fibers could be acting as if they were wider, thus triggering a determination of a lower aspect ratio.

Finally, two morphological parameters have been considered: first, a branching index indicates the proportion of nodes found in the skeleton of fibers to the projected area [26]; second, the 2D fractal dimension refers to the compacity of the fibers, quantified also in the images [58]. As observed, BKSP has a higher branching index and fractal dimension than BKHP. Attending to the microscopy images in Table 1, BKSP fibers are quite peeled compared to BKHP fibers, which present a smooth and homogeneous surface. This reason has been again attributed to the different crystallinity and crystalline dimensions observed in both samples: the longer and more abundant crystals of BKSP could have triggered a stiffer behavior when pulps are submitted to mechanical stresses [59], hence causing the breaking of some fibrils that remained attached to the fiber backbone.

The composition of the pretreated samples after mechanical (refining), enzymatic hydrolysis and TEMPO-mediated oxidation has been also evaluated (Fig. 2). Neither mechanical pretreatment nor enzymatic hydrolysis (H80 and H240) had a perceptible effect over the sample composition. However, samples pretreated through TEMPO-mediated oxidation (T5 and T15) varied in a higher proportion compared to the others and in a special way in T15-CNFs. Three different behaviors can be described. First and foremost, the strong conditions of TEMPO-mediated oxidation make the dissolution of a part of the amorphous cellulose fractions [32]. This loss of cellulose causes the rest of the components increase, mainly the hemicellulose, because it is the second majority component. On the other hand, although it is more difficult to see as lignin is a minority compound due to is mostly removed in bleaching, the lignin content slightly decreased on both BKSP and BKHP samples. This fact can be clearly attributed to the presence of NaClO, and even more when NaClO is coupled with TEMPO-mediated oxidation catalysts [60]. Finally, ash content, which had negligible values in the rest of the pulps, started to increase considerably in a direct manner related to the amount of NaClO. Since the percentages were approximately the same in both pulps, BKSP and BKHP, this effect

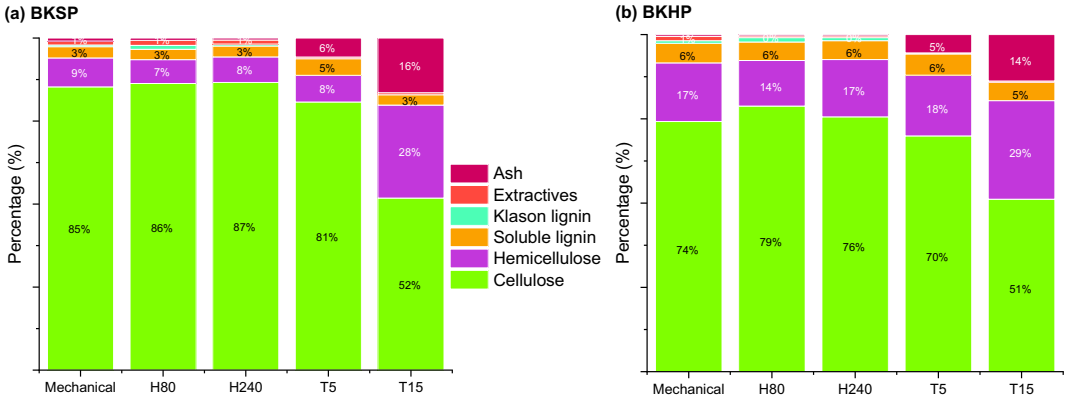

Fig. 2. Compositional analysis of the pretreated samples.

was attributed to some residual salts derived from the oxidation reaction. Two main reasons could have governed this behavior: first, the oxidation reaction gives NaCl as a product [13], that could have remained attached to the fibers even after washing. Second, some industries have generally added NaCl to the commercial NaClO just to improve its stability during storage [61], and this low proportion could have remained also together with the fibers. An additional variable could be the fact that some cellulose fibrils could have been dissolved or stabilized in a colloidal form after oxidation reaction, which could have caused the breaking of some pieces of cellulose caused by an excessive electrostatic repulsion between carboxyl groups. This small fraction could have been lost during washing, reducing the amount of cellulose from the total composition.

Finally, the effect that each pretreatment had on the initial sources was analyzed in terms of physicochemical properties and morphological parameters (Table 2). Carboxyl content was only modified with the TEMPO-mediated oxidation reaction, and reached a constant value in both cellulose sources, which was directly related to the oxidant dose. CrI also increased in a higher way with TEMPO pretreatment due to part of the amorphous cellulose is dissolved in the reaction medium [62], while in the rest of pretreatments there are hardly any variation with respect to the raw material, maintaining the proportion between amorphous and crystalline regions.

Regarding morphology, a different behavior was observed in both samples. In mechanically pretreated pulps, both branching index and aspect ratio increased, whose reason was mainly attributed to the separation of the fibers by intensive shear stress. Fig. 3 proposes a schematic diagram of the effect of each pretreatment. In the case of enzymatic hydrolysis, the breaking of the cellulose chains, mainly in the amorphous region, produces the decrease of the aspect ratio, similarly in both raw materials but having different branching index. A higher value in this parameter was found for BKSP, which could be due to the higher initial branching aspect of the pulp, but also to a higher breaking of the fibrils caused by the characteristic stiffness of this material.

Finally, although the final oxidation degree of both pretreated pulps with TEMPO-mediated oxidation was similar in terms of carboxyl groups, the morphology resulted to be very different. As explained in a previous publication [13], once the pulp has been oxidized at a certain point, the electrostatic repulsion induced by the carboxyl groups causes the breaking of the fibers in those areas close to the crystalline regions. Thus, it makes sense to think that this breaking would reach a higher degree in the pulps with longer crystallites, i.e. BKSP.

3.2. Study of CNF homogeneity

Homogeneity of CNFs is an important factor when using them for a particular application. When a sample has been highly fibrillated, meaning that the minimum possible diameter is reached, the suspension becomes optically transparent at test concentration (0.1 wt%), i.e. with a transmittance near to 100% [63]. On the other hand, it is common to find that some authors used the nanofibrillation yield to determine the

Table 2
Characterization of pretreated materials.

Raw material	Pretreatment	Carboxyl groups (μeq/g)	Crystallinity Index (%)	Branching index (μm^{-2})	Aspect ratio
BKSP	Mechanical	53	78.4	$5.82 \cdot 10^{-4}$	118
	H80	53	80.7	$4.78 \cdot 10^{-4}$	53
	H240	53	81.0	$3.65 \cdot 10^{-4}$	47
	T5	816	84.9	$3.35 \cdot 10^{-4}$	59
	T15	1374	87.0	$3.70 \cdot 10^{-4}$	35
BKHP	Mechanical	44	71.1	$3.92 \cdot 10^{-4}$	110
	H80	45	69.9	$2.58 \cdot 10^{-4}$	61
	H240	45	72.9	$3.28 \cdot 10^{-4}$	65
	T5	821	73.3	$1.71 \cdot 10^{-4}$	47
	T15	1385	75.1	$4.01 \cdot 10^{-4}$	42

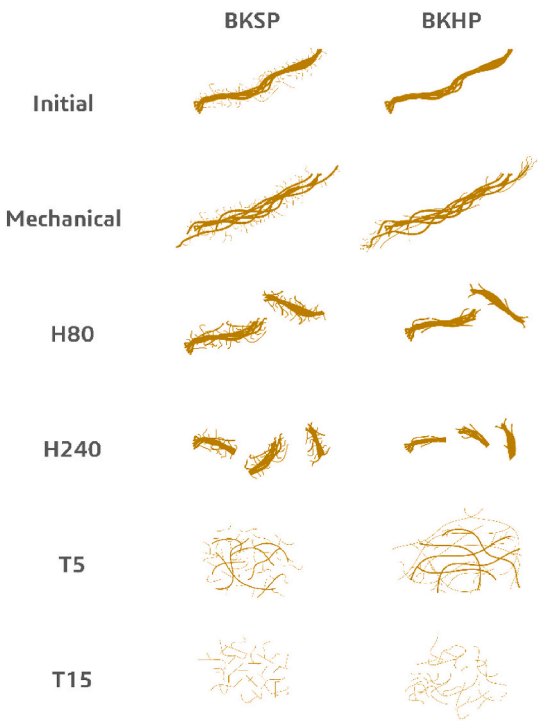

Fig. 3. Schematic representation of the morphology of pretreated samples.

degree of homogeneity of the sample, measured as the ratio between fibrillated and non-fibrillated fractions determined by centrifugation. Like transmittance, a higher nanofibrillation yield would indicate a higher number of fibers in the nanometric scale. Therefore, a smaller average diameter of the fibers is expected. Fig. 4 shows the evolution of transmittance vs nanofibrillation yield and shows an almost total proportionality for all CNFs obtaining a R^2 over 0.995. Both raw materials present the same fitting indicating that neither the cellulose source nor the treatments disrupt the relation between both properties. According to the literature, others raw materials as Aspen cellulose present the same behavior [43]. Therefore, the evaluation of both characteristics proportionate comparable information and in an industrial perspective, transmittance would be the most affordable parameter since it would require less-time consuming and low cost equipment, due to fact that centrifugation is not required [8].

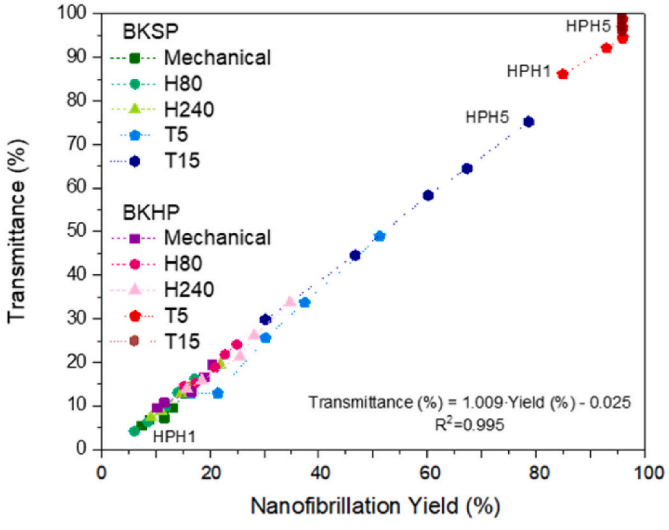

Fig. 4. Relationship between transmittance and nanofibrillation yield of CNFs.

As for the surface charge, it becomes higher when all nanofibrils have been released, having the whole surface full of hydroxyl groups with a negative charge [64]. At this point CD reach the highest value. Fig. 5 shows the evolution of transmittance as function of the CD of CNF samples. We have solely considered in this study the transmittance values to make the comparison with CD due to the scarce differences with nanofibrillation yield (Fig. 4). Mechanical treatment induced higher fibrillation in BKHP compared to BKSP, with higher CD and transmittance of CNFs that are obtained using the same homogenization sequence. In addition, there is an increment in both parameters with the intensity of the homogenization process. Although there were clear differences between the evolution of these parameters in both raw materials, they seldom varied when the enzyme dose was increased (from H80 to H240). CD and transmittance started in almost the same point (HPH1) in both enzymatic pretreatments with the same raw material, with higher values of CD than in mechanically treated HPH1. However, HPH caused a higher effect in H240 samples, when both parameters were compared in HPH1 and HPH5. A higher homogeneity in the fibrillated product was achieved in BKHP samples and could be due to the higher efficiency of enzymes to hydrolyze amorphous cellulose [65]. Nevertheless, none of the samples got transmittance values over 35%, indicating that some of the fibers still have a macroscopic size, as observed in TEM images (Fig. 6).

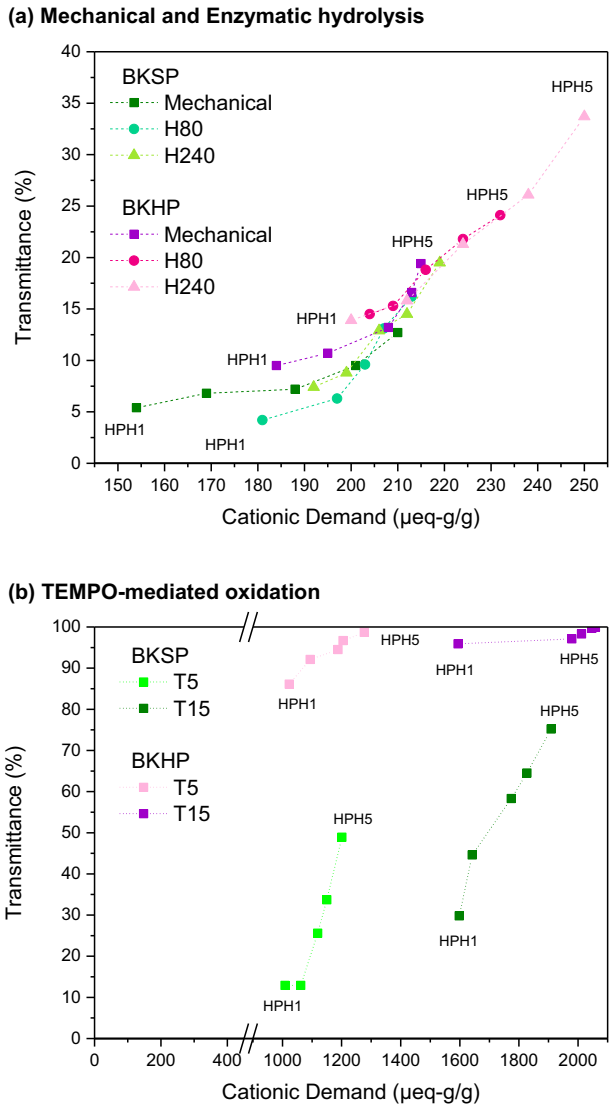

Fig. 5. Relationship between transmittance and cationic demand of CNFs.

TEMPO-mediated oxidation had a similar effect on CD of samples depending on the oxidant dose, having a value of around 1000 μeq/g in the case of HPH1 pretreated with T5 and 1600 μeq/g in the case of HPH1 pretreated with T15 (Fig. 5b). Great part of this value is due to the increase in the carboxyl groups in C6 of cellulose. However, values in transmittance were more significantly similar by raw material. In BKHP samples, almost 100% of transmittance was achieved, while the maximum transmittance value observed in BKSP was 75% with T15 and HPH5. This fact may be due to the higher hemicellulose content of BKHP samples, that produces an easier nanofibrillation of the fibers, since the hemicellulose acts as a physical barrier between fibers reducing the extension of microfibrils aggregates and the amount of intrafibrillar hydrogen bonding [55,66,67]. In addition, the differences in both crystallinity and crystallite size of the raw materials, both higher in BKSP samples, may also influence in the differences observed in transmittance between the two sources. Most amorphous areas may have been oxidized and due to the dramatic shift in the electrostatic charge and the high resistance of crystalline areas to be unmodified [68], many of the cellulose chains could have been broken instead of hydrolyzed. This difference in the morphology of samples, which gave place to a difference in transmittance values, was also observed in TEM images of Fig. 6.

3.3. Rheological behavior of CNFs

Flow behavior is one of the most important factors in the application of CNFs and its variation may be due to several factors, such as the hemicellulose content that try to keep the fibers glued or the substitution of hydroxyl groups by charged ions as in TEMPO pretreatment, promoting stronger electrostatic repulsion and increasing suspension stability [69]. The apparent viscosity as a function of shear rate is logarithmically plotted in Fig. 7 for the different HPH sequences and pretreatments. The representation of the apparent viscosity as function of the shear rate of several samples provides useful information on the fluid characteristics. For instance, two evolutions exhibiting a similar slope (flow behavior index, n) but differences on the apparent viscosity at certain shear rate, indicates differences on the consistency index (K), which depend on the individual fiber characteristics and can vary in several order of magnitude [47,70,71]. Newtonian fluids maintain the proportion viscosity with shear rate with n equal to 1. On the other hand, when n is below 1, as it is the case of CNF suspensions (Fig. 7), the behavior is pseudo-plastic [72].

The rheological behavior of CNFs is a complex system influenced by multiple parameters, such as the CNF entanglement, the ramification, their aspect ratio, the concentration, their composition or the specific surface area, among others [47]. Comparing BKSP and BKHP CNFs with mechanical pretreatment, a higher K is obtained in BKSP associated with a higher ramification [26], already from the raw material, as TEM micrographs shown in Fig. 6 and Table 1. The initial ramification of BKSP makes that despite having higher viscosity values, the increase with the HPH severity be scarce. However, BKHP with a smooth surface and a reduce branching, despite having less viscosity, the effect of HPH produce a higher variation of viscosity which indicates more effectivity on the homogenization. In this sense, the transmittance of BKHP also showed in Fig. 4 a greater variation from HPH1 to HPH5 in this source. Moving on to enzymatic CNFs, the shortening in the pretreatment reduce the entanglement of the fibers, which produces lower viscosity than mechanically pretreated samples. Comparing raw materials, both present minor differences, but the initial smooth surface of BKHP makes the viscosity slightly lower. Comparing both doses of enzymes, the higher dose, H240-CNFs show higher variation in viscosity, so the HPH produces more effectivity in this property and in a greater way in BKHP as occurs with mechanical CNFs. That is why, as a summary, both pretreatments, despite BKSP having a higher viscosity due to its fibrillation, BKHP shows greater effectiveness with the treatments performed. On the other hand, CNFs pretreated with TEMPO-mediated oxidation

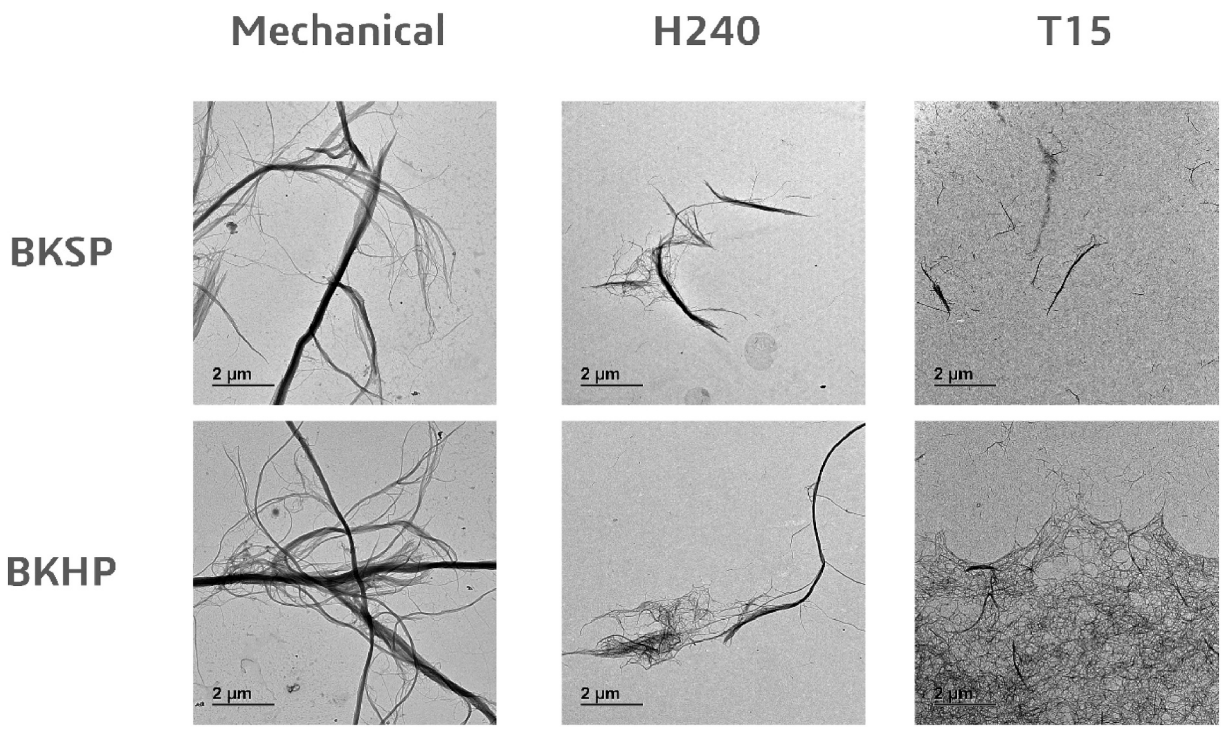

Fig. 6. TEM images of HPH5 samples of both raw materials with the three pretreatments.

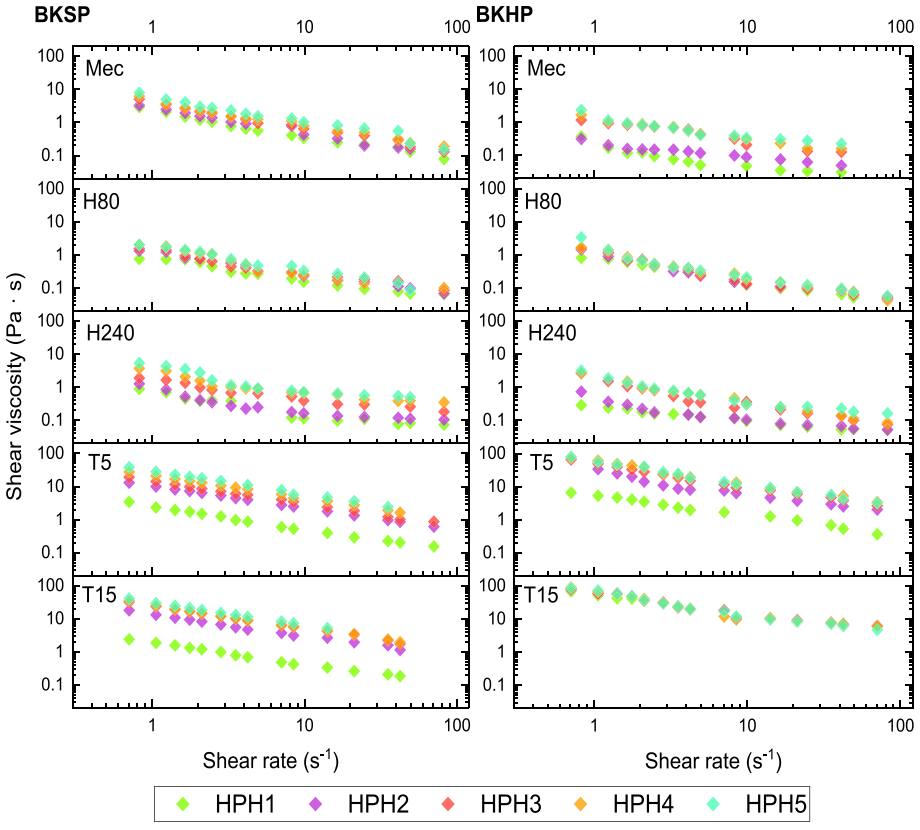

Fig. 7. Comparison of apparent viscosity vs shear rate for different treatments and pretreatments.

BKHP-CNFs have higher apparent viscosity. The great severity of this pretreatment produces the oxidation of cellulose introducing carboxyl groups that increase the electrostatic charge of the fibrils, which causes the dissipation of some of the amorphous regions reducing the chain size of cellulose [73]. Therefore, the BKSP oxidized with TEMPO procedure, show the separation of branched fibrils from the primary structures, observing small fibers with low aspect ratio even some of them with nanocrystals morphology at high doses of NaClO [74]. Additionally to

the initial branching morphology of this pulp, the lower hemicellulose content of BKSP that typically acts to hold the fibers together made this pulp easier to fibrillate [55]. However, BKHP contains a higher amount of hemicellulose that difficult the completely break of the fibers forming a kind of network instead of separating the fibers, which increases viscosity and *K* in a higher extent than in BKSP [75].

Fig. 7 also shows an increase in apparent viscosity with the homogenization intensity during the shear rate range analyzed and for all pretreatments. This viscosity variation in the application of different HPH sequences is more accused in TEMPO samples, in which after a low number of passes (from HPH2) a gel structure, more viscous, is observed. Only BKHP pretreated with T15 directly shows a high viscosity of all samples from HPH1. Therefore, 3 passes of homogenization at 300 bar are enough to obtain viscous CNF suspensions with high transmittance, not being necessary a more severe treatment.

As for the flow behavior index, this parameter shows a very slight decrease with homogenization severity which indicates a higher pseudoplastic behavior of these CNFs. However, the comparison of flow behavior index must be evaluated cautiously due to the possible presence of slip flow, a lubricating layer adjacent to the rheometer walls where the CNF loss adhesion producing higher viscosity values, mainly at high shear rates [76,77]. Therefore, one way to identify the slip flow in the logarithmic representation of apparent viscosity in front of shear rate is the curvature of the plot instead of a line, in which the last values can be affected by this effect that increase the flow behavior index even above 200% [76]. This effect is clearly observed in H240 samples for both raw materials in which flow index is notably reduced when the fits are carried out with shear rates under 5 s^{-1}, improving R^2 and maintaining the consistency index.

3.4. Comparison of rheological and morphological parameters

CNFs and CNCs from different raw materials, treatments and pretreatments show a wide variety of parameters related to composition, morphology, and rheology [75]. Therefore, the selection of the most adequate CNFs is key for each application: for instance, rheology is essential in applications like coating or 3D printing, requiring a high CNF concentration; in other applications, including food thickener or in the production of composites, the rheology is also important but concentration will depend on the final use [78]. On the other hand, morphology parameters could be key, such as the entanglement of the fibers in the production of aerogels [79].

Thus, the comparison of microscopic parameters as fractal dimension and branching index to characterize the morphology of the samples with macroscopic parameters as the aspect ratio, determined through a bulk behavior, or the consistency index parameter could be the most useful to select the more adequate raw materials and treatments. One of the possible comparisons is shown in Fig. 8, which relates *K* with aspect ratio for all pretreatments. We consider *K* instead of *n* as representant of rheology, since *n* flow index may present discrepancies associated to the slip flow of the suspensions, which would difficult the analysis [76]. On the other hand, fractal dimension pretends to be a very useful tool to estimate the irregularity of fibers. Fig. 8a shows that fractal dimension of CNFs is practically invariable with mechanical pretreatment. With the severity of homogenization, *K* increases while the compactness of the primary structures (fractal dimension) is maintained in both samples with a slightly higher fractal dimension in BKSP associated with the higher ramification. On the other hand, enzymatic pretreatment produces higher variation in fractal dimension of CNFs whereas the consistency index scarce increase. The shortening of the fibers with the pretreatment is observed in HPH1 for both samples and doses, with lower values of fractal dimension than mechanical CNFs. However, increasing HPH severity the shortening stop being observed due to the peeling of the fibers and the presence of microfibrils around the primary structures, producing the reverse effect an increasing fractal dimension values. However, fractal dimension decreased again when these microfibrils separate totally from the bundles of fibers at higher HPH severity.

This fact is also observed in Fig. 8b with TEMPO-mediated oxidation pretreatment, the separation of the fibers and breakage of the chains produce the reduction of the fractal dimension. This effect is more remarkable in BKSP with lower fractal dimension values after both doses of oxidation. From this raw material is possible to observe some CNC structures among the fibers after T15 as Fig. 6 shows, whereas in BKHP a network structure is maintained, and fractal dimension stays at higher values. However, the presence of still CNFs in BKSP-T15 can cause the non-decrease of *K* as occurred in woody plants, i.e. sisal and hemp, in which the strong oxidation conditions produce the breakage of the most part of CNFs to CNCs, reducing *K*, even more with the homogenization sequence that still breaks more the material [32].

Fig. 9 compares aspect ratio and branching index for all pretreatments. The aspect ratio of some T15-CNFs has not been possible to be measured due to the lack of deposits in the gel point measurement, mainly in T15-BKHP. This is justified by the high viscosity of the samples that may hinder the CNF deposition together with the slow sedimentation process and the small deposit produced. Only BKSP with T15 and HPH1 and HPH2 were registered with aspect ratio under 10, suggesting the obtention of CNCs [74]. On the other hand, only OM images were

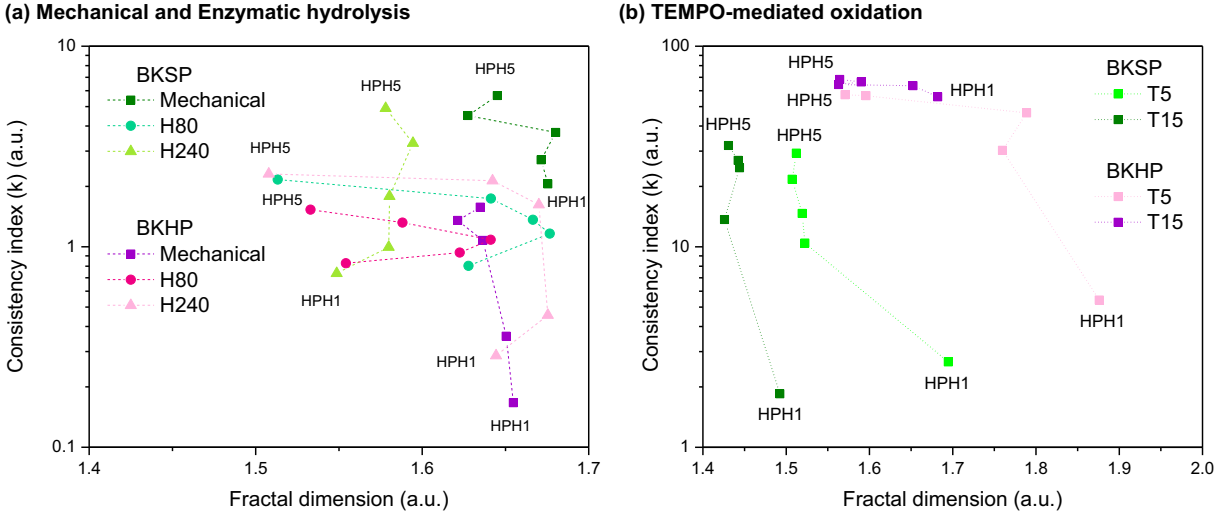

Fig. 8. Relationship between consistency index (K) and fractal dimension of CNFs.

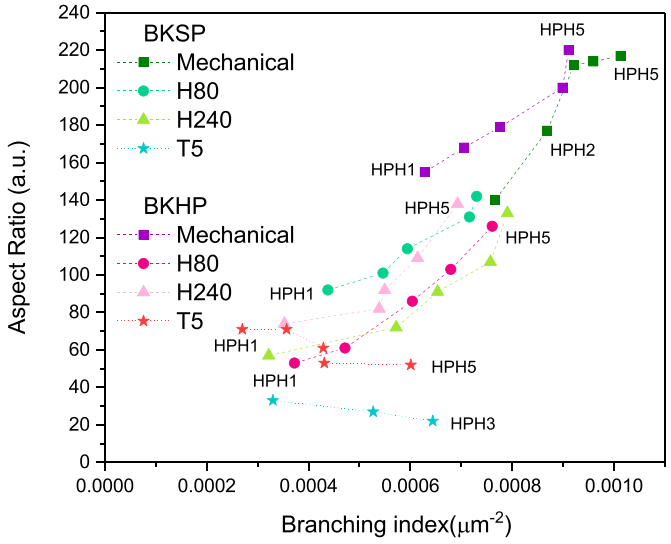

Fig. 9. Aspect ratio vs branching index.

selected to calculate branching index. By the same way than in OM, this technique also could be used in TEM images, obtaining results in another scale. However, the low number of aspect ratio values obtained in T15 samples makes there few samples to compare.

In general, CNFs from both sources pretreated with mechanical and enzymatic hydrolysis do not show high differences in aspect ratio, only in both cases an increase it with the HPH severity, due to the reduction of the diameter of the fibers with the peeling of them, forming secondary fibers. On the other hand, branching index, which gives an idea of the ramification of the samples, shows after mechanical pretreatment a higher value in BKSP than BKHP due to a higher crystallinity of BKSP which makes that after the application of mechanical strengths the microfibrils peeled remain attached to the primary fibers. After enzymatical pretreatment, branching index is not as high as in refining due to the shortening of the fibers in this pretreatment, presenting similar results for both samples, slightly higher in BKSP due to the raw materials was initially more branched. However, TEMPO-mediated oxidation produces a reverse effect in aspect ratio, which is reduced with HPH. This fact is due to the predominance of the fiber split during homogenization associated with the break of β-1,4 glycosidic bonds in the cellulose chains after TEMPO-mediated oxidation [13]. This shortening becomes more effective the more pressure is applied to the homogenizer, until the samples are not observable in the OM, therefore branching index cannot be measured in BKSP-T5 with HPH4 and HPH5. BKSP present smaller aspect ratios associated to the high effect of TEMPO-mediated oxidation in this raw material, may be due to several factors as lower contents of lignin and hemicellulose that make the NaClO dedicates completely to oxidize the cellulose or the nature of the raw material with higher peeling of the microfibrils that facilitate the break of the fibrils [26,60].

To sum up, the effect of the chemical composition, and morphological and rheological parameters developed in this study have been collected in a simplified way by a color code in Fig. 10. The increase or decrease of each property is easily observed according to the raw material, pretreatment and treatment intensity. In such a way that depending on the parameter for which it is required to obtain a high or low value, it is possible to select the source and treatments to prepare the CNFs.

4. Conclusions

CNFs produced from BKSP and BKHP showed very diverse properties, regarding structural, morphological, and rheological behavior. This article settled, in a critical comparison, the main features of the raw materials that affect to the effectivity of both the pretreatments and the treatments used to produce CNFs. The different types and amounts of hemicelluloses and lignin presented in both types of wood caused that bleached kraft pulps triggered a significant effect on the nanofibrillation process. The different crystallinity and crystal size of cellulose marked the changes in morphology of CNFs and their rheological behavior obtained after each treatment. BKHP fibers, which have a higher content of amorphous cellulose, were more prone to keep the fibrillar structure as shown by the transmittance, the nanofibrillation yield and the fractal dimension. On the other hand, BKSP fibrils tended to break more easily. This effect is also denoted by the rheology data that shows a higher variation in BKHP samples after the increase in HPH severity, despite the higher global values obtained in mechanical and enzymatic BKSP that are associated to the initial branching. These results will facilitate researchers and industries to select the most adequate and effective raw

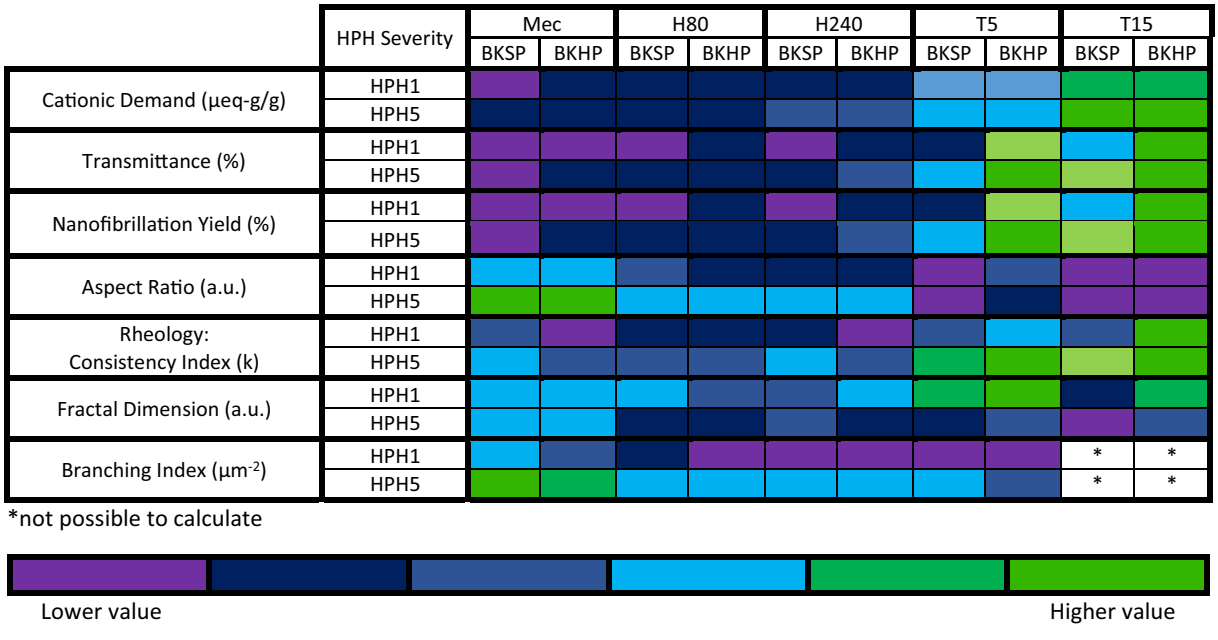

Fig. 10. Summary of chemical, morphological and rheological measurements.

material and procedure to obtain fit-for-use CNFs for a given application.

CRediT authorship contribution statement

- Authors declare that in this work we have not involve any human subjects.
- Authors declare no competing interests.
- Authors declare we have read the information on Ethics in publishing.
- Sample CRediT author statement:

  JL. Sanchez-Salvador: Investigation, Conceptualization, Formal analysis, Writing – Original Draft; C. Campano: Investigation, Methodology, Formal analysis, Writing – Original Draft; A. Balea: Visualization, Investigation, Writing – Review & Editing; Q. Tarres: Methodology, Supervision, Writing – Review & Editing; M. Delgado-Aguilar: Supervision, Project administration, Writing – Review & Editing; P. Mutje: Funding acquisition, Writing – Review & Editing; A. Blanco: Supervision, Resources, Writing – Review & Editing; C. Negro: Conceptualization; Project administration, Funding acquisition, Writing – Review & Editing.

Acknowledgments

Authors want to acknowledge the Spanish Ministry of Economy and Competitiveness for the funding of the projects CTQ2017-85654-C2-1-R and CTQ2017-85654-C2-2-R, the Spanish Ministry of Science and Innovation (PDC2021-120964-C21 and PDC2021-120964-C22), the Community of Madrid for funding the RETO-PROSOST-2-CM (P2018/EMT4459), as well as the support of Universidad Complutense de Madrid and Banco de Santander for the grant of J.L. Sanchez-Salvador (CT17/17). Thanks also to Spanish Ministry of Science and Innovation for the Juan de la Cierva aid of Cristina Campano (Ref. FJC2019-040298-I). Finally, thanks to the Spanish National Centre of Electronic Microscopy for the support during image acquisition. Marc Delgado-Aguilar is a Serra Húnter Fellow.

References

[1] J. Zhang, D. Cai, Y. Qin, D. Liu, X. Zhao, High value-added monomer chemicals and functional bio-based materials derived from polymeric components of lignocellulose by organosolv fractionation, Biofuels Bioprod. Biorefin. 14 (2) (2020) 371–401.
[2] A. Blanco, M.C. Monte, C. Campano, A. Balea, N. Merayo, C. Negro, in: Nanocellulose for Industrial Use: Cellulose Nanofibers (CNF), Cellulose Nanocrystals (CNC), and Bacterial Cellulose (BC), Handbook of Nanomaterials for Industrial Applications, Elsevier, 2018, pp. 74–126.
[3] O. Nechyporchuk, M.N. Belgacem, J. Bras, Production of cellulose nanofibrils: a review of recent advances, Ind. Crop. Prod. 93 (2016) 2–25.
[4] S.P. Chundawat, B.S. Donohoe, L. da Costa Sousa, T. Elder, U.P. Agarwal, F. Lu, J. Ralph, M.E. Himmel, V. Balan, B.E. Dale, Multi-scale visualization and characterization of lignocellulosic plant cell wall deconstruction during thermochemical pretreatment, Energy Environ. Sci. 4 (3) (2011) 973–984.
[5] M. He, G. Yang, J. Chen, X. Ji, Q. Wang, Production and characterization of cellulose nanofibrils from different chemical and mechanical pulps, J. Wood Chem. Technol. 38 (2) (2018) 149–158.
[6] M. Kaur, P. Sharma, S. Kumari, State of art manufacturing and producing nanocellulose from agricultural waste: a review, J. Nanosci. Nanotechnol. 21 (6) (2021) 3394–3403.
[7] M. Asyraf, M. Rafidah, A. Azrina, M. Razman, Dynamic mechanical behaviour of kenaf cellulosic fibre biocomposites: a comprehensive review on chemical treatments, Cellulose (2021) 1–21.
[8] C. Moser, M.E. Lindström, G. Henriksson, Toward industrially feasible methods for following the process of manufacturing cellulose nanofibers, Bioresources 10 (2) (2015) 2360–2375.
[9] A. Pandey, Pharmaceutical and biomedical applications of cellulose nanofibers: a review, Environ. Chem. Lett. (2021) 1–13.
[10] B. Poyraz, A. Tozluoğlu, Z. Candan, A. Demir, M. Yavuz, Ü. Büyuksarı, H.İ. Ünal, H. Fidan, R.C. Saka, TEMPO-treated CNF composites: pulp and matrix effect, Fibers Polym. 19 (1) (2018) 195–204.
[11] L. Alves, E. Ferraz, A. Lourenço, P. Ferreira, M. Rasteiro, J. Gamelas, Tuning rheology and aggregation behaviour of TEMPO-oxidised cellulose nanofibrils aqueous suspensions by addition of different acids, Carbohydr. Polym. 237 (2020), 116109.
[12] A. Dijksman, A. Marino-González, A. Mairata i Payeras, I.W. Arends, R.A. Sheldon, Efficient and selective aerobic oxidation of alcohols into aldehydes and ketones using ruthenium/TEMPO as the catalytic system, J. Am. Chem. Soc. 123 (28) (2001) 6826–6833.
[13] J.L. Sanchez-Salvador, C. Campano, C. Negro, M.C. Monte, A. Blanco, Increasing the possibilities of TEMPO-mediated oxidation in the production of cellulose nanofibers by reducing the reaction time and reusing the reaction medium, Adv. Sustain. Syst. 5 (4) (2021), 2000277.
[14] X. Sun, Q. Wu, S. Ren, T. Lei, Comparison of highly transparent all-cellulose nanopaper prepared using sulfuric acid and TEMPO-mediated oxidation methods, Cellulose 22 (2) (2015) 1123–1133.
[15] Y. Chen, B. Geng, J. Ru, C. Tong, H. Liu, J. Chen, Comparative characteristics of TEMPO-oxidized cellulose nanofibers and resulting nanopapers from bamboo, softwood, and hardwood pulps, Cellulose 24 (11) (2017) 4831–4844.
[16] J. Moohan, S.A. Stewart, E. Espinosa, A. Rosal, A. Rodríguez, E. Larrañeta, R. F. Donnelly, J. Domínguez-Robles, Cellulose nanofibers and other biopolymers for biomedical applications. A review, Appl. Sci. 10 (1) (2020) 65.
[17] S. Gwon, Y.C. Choi, M. Shin, Effect of plant cellulose microfibers on hydration of cement composites, Constr. Build. Mater. 267 (2021), 121734.
[18] F. Masoudzadeh, M. Fasihi, M. Jamshidi, The influence of cellulose pulp and cellulose microfibers on the flexural performance of green-engineered cementitious composites, J. Part. Sci. Technol. 3 (1) (2017) 33–40.
[19] J.L. Sanchez-Salvador, A. Balea, M.C. Monte, C. Negro, M. Miller, J. Olson, A. Blanco, Comparison of mechanical and chemical nanocellulose as additives to reinforce recycled cardboard, Sci. Rep. 10 (1) (2020) 3778.
[20] Q. Tarrés, S. Boufi, P. Mutjé, M. Delgado-Aguilar, Enzymatically hydrolyzed and TEMPO-oxidized cellulose nanofibers for the production of nanopapers: morphological, optical, thermal and mechanical properties, Cellulose 24 (9) (2017) 3943–3954.
[21] H. Seddiqi, E. Oliaei, H. Honarkar, J. Jin, L.C. Geonzon, R.G. Bacabac, J. Klein-Nulend, Cellulose and its derivatives: towards biomedical applications, Cellulose (2021) 1–39.
[22] Y. Zhao, C. Moser, M.E. Lindström, G. Henriksson, J. Li, Cellulose nanofibers from softwood, hardwood, and tunicate: preparation–structure–film performance interrelation, ACS Appl. Mater. Interfaces 9 (15) (2017) 13508–13519.
[23] C. Tengborg, K. Stenberg, M. Galbe, G. Zacchi, S. Larsson, E. Palmqvist, B. Hahn-Hägerdal, Comparison of SO 2 and H 2 SO 4 impregnation of softwood prior to steam pretreatment on ethanol production, Appl. Biochem. Biotechnol. 70 (1) (1998) 3–15.
[24] W. Stelte, A.R. Sanadi, Preparation and characterization of cellulose nanofibers from two commercial hardwood and softwood pulps, Ind. Eng. Chem. Res. 48 (24) (2009) 11211–11219.
[25] K. Syverud, G. Chinga-Carrasco, J. Toledo, P.G. Toledo, A comparative study of eucalyptus and Pinus radiata pulp fibres as raw materials for production of cellulose nanofibrils, Carbohydr. Polym. 84 (3) (2011) 1033–1038.
[26] J.L. Sanchez-Salvador, C. Campano, P. Lopez-Exposito, Q. Tarrés, P. Mutjé, M. Delgado-Aguilar, M.C. Monte, A. Blanco, Enhanced morphological characterization of cellulose nano/microfibers through image skeleton analysis, Nanomaterials-Basel 11 (8) (2021) 2077.
[27] A. Balea, N. Merayo, E. De La Fuente, C. Negro, A. Blanco, Assessing the influence of refining, bleaching and TEMPO-mediated oxidation on the production of more sustainable cellulose nanofibers and their application as paper additives, Ind. Crop. Prod. 97 (2017) 374–387.
[28] B. Deepa, E. Abraham, N. Cordeiro, M. Faria, G. Primc, Y. Pottathara, M. Leskovšek, M. Gorjanc, M. Mozetič, S. Thomas, Nanofibrils vs nanocrystals bio-nanocomposites based on sodium alginate matrix: an improved-performance study, Heliyon 6 (2) (2020), e03266.
[29] A.J. Onyianta, M. Dorris, R.L. Williams, Aqueous morpholine pre-treatment in cellulose nanofibril (CNF) production: comparison with carboxymethylation and TEMPO oxidisation pre-treatment methods, Cellulose 25 (2) (2018) 1047–1064.
[30] M. Jonoobi, A. Khazaeian, P.M. Tahir, S.S. Azry, K. Oksman, Characteristics of cellulose nanofibers isolated from rubberwood and empty fruit bunches of oil palm using chemo-mechanical process, Cellulose 18 (4) (2011) 1085–1095.
[31] J. Zeng, F. Hu, Z. Cheng, B. Wang, K. Chen, Isolation and rheological characterization of cellulose nanofibrils (CNFs) produced by microfluidic homogenization, ball-milling, grinding and refining, Cellulose 28 (6) (2021) 3389–3408.
[32] F. Serra-Parareda, Q. Tarrés, J.L. Sanchez-Salvador, C. Campano, M.À. Pèlach, P. Mutjé, C. Negro, M. Delgado-Aguilar, Tuning morphology and structure of non-woody nanocellulose: ranging between nanofibers and nanocrystals, Ind. Crop. Prod. 171 (2021), 113877.
[33] A. Isogai, T. Saito, H. Fukuzumi, TEMPO-oxidized cellulose nanofibers, Nanoscale 3 (1) (2011) 71–85.
[34] C. Campano, N. Merayo, A. Balea, Q. Tarres, M. Delgado-Aguilar, P. Mutje, C. Negro, A. Blanco, Mechanical and chemical dispersion of nanocelluloses to improve their reinforcing effect on recycled paper, Cellulose 25 (1) (2018) 269–280.
[35] L. Segal, J. Creely, A. Martin Jr., C. Conrad, An empirical method for estimating the degree of crystallinity of native cellulose using the X-ray diffractometer, Text. Res. J. 29 (10) (1959) 786–794.
[36] C. Campano, A. Balea, Á. Blanco, C. Negro, A reproducible method to characterize the bulk morphology of cellulose nanocrystals and nanofibers by transmission electron microscopy, Cellulose 27 (9) (2020) 4871–4887.
[37] M. Delgado-Aguilar, I. Gonzalez, Q. Tarres, M. Alcala, M.A. Pelach, P. Mutje, Approaching a low-cost production of cellulose nanofibers for papermaking applications, Bioresources 10 (3) (2015) 5345–5355.

[38] J.L. Sanchez-Salvador, M.C. Monte, C. Negro, W. Batchelor, G. Garnier, A. Blanco, Simplification of gel point characterization of cellulose nano and microfiber suspensions, Cellulose (2021) 1–12.
[39] J.L. Sanchez-Salvador, M.C. Monte, W. Batchelor, G. Garnier, C. Negro, A. Blanco, Characterizing highly fibrillated nanocellulose by modifying the gel point methodology, Carbohydr. Polym. 227 (2020), 115340.
[40] S. Varanasi, R. He, W. Batchelor, Estimation of cellulose nanofibre aspect ratio from measurements of fibre suspension gel point, Cellulose 20 (4) (2013) 1885–1896.
[41] D. Martinez, K. Buckley, S. Jivan, A. Lindstrom, R. Thiruvengadaswamy, J. Olson, T. Ruth, R. Kerekes, Characterizing the mobility of papermaking fibres during sedimentation, in: The Science of Papermaking: Transactions of the 12th Fundamental Research Symposium, Oxford. The Pulp and Paper Fundamental Research Society, Bury, UK, 2001, pp. 225–254.
[42] A. Balea, J.L. Sanchez-Salvador, M.C. Monte, N. Merayo, C. Negro, A. Blanco, In situ production and application of cellulose nanofibers to improve recycled paper production, Molecules 24 (9) (2019).
[43] A. Balea, Q. Tarrés, M. Pèlach, P. Mutjé, M. Delgado-Aguilar, A. Blanco, C. Negro, Influence of pretreatment and mechanical nanofibrillation energy on properties of nanofibers from Aspen cellulose, Cellulose 28 (14) (2021) 9187–9206.
[44] C. Campano, P. Lopez-Exposito, L. Gonzalez-Aguilera, Á. Blanco, C. Negro, In-depth characterization of the aggregation state of cellulose nanocrystals through analysis of transmission electron microscopy images, Carbohydr. Polym. 254 (2021), 117271.
[45] C. Campano, P. Lopez-Exposito, L. Gonzalez-Aguilera, Á. Blanco, C. Negro, In-depth characterization of the aggregation state of cellulose nanocrystals through analysis of transmission electron microscopy images, Carbohydr. Polym. 117271 (2020).
[46] M. Mohtaschemi, A. Sorvari, A. Puisto, M. Nuopponen, J. Seppälä, M.J. Alava, The vane method and kinetic modeling: shear rheology of nanofibrillated cellulose suspensions, Cellulose 21 (6) (2014) 3913–3925.
[47] A.I. Koponen, The effect of consistency on the shear rheology of aqueous suspensions of cellulose micro-and nanofibrils: a review, Cellulose 27 (4) (2020) 1879–1897.
[48] I. Filipova, F. Serra, Q. Tarres, P. Mutje, M. Delgado-Aguilar, Oxidative treatments for cellulose nanofibers production: a comparative study between TEMPO-mediated and ammonium persulfate oxidation, Cellulose 27 (18) (2020) 10671–10688.
[49] A. Kumagai, T. Endo, Effects of hemicellulose composition and content on the interaction between cellulose nanofibers, Cellulose 28 (1) (2021) 259–271.
[50] R.B. Santos, E.A. Capanema, M.Y. Balakshin, H.-M. Chang, H. Jameel, Effect of hardwoods characteristics on Kraft pulping process: emphasis on lignin structure, Bioresources 6 (4) (2011) 3623–3637.
[51] T.G. Van De Ven, A. Sheikhi, Hairy cellulose nanocrystalloids: a novel class of nanocellulose, Nanoscale 8 (33) (2016) 15101–15114.
[52] J. Laine, P. Stenius, Effect of charge on the fibre and paper properties of bleached industrial Kraft pulps, Paperi Ja Puu-PaperTimber 79 (4) (1997) 257–266.
[53] E. Sjöholm, K. Gustafsson, F. Berthold, A. Colmsjö, Influence of the carbohydrate composition on the molecular weight distribution of Kraft pulps, Carbohydr. Polym. 41 (1) (2000) 1–7.
[54] K.L. Spence, R.A. Venditti, Y. Habibi, O.J. Rojas, J.J. Pawlak, The effect of chemical composition on microfibrillar cellulose films from wood pulps: mechanical processing and physical properties, Bioresour. Technol. 101 (15) (2010) 5961–5968.
[55] A. Andrade, S. Henríquez-Gallegos, G. Albornoz-Palma, M. Pereira, Effect of the chemical and structural characteristics of pulps of eucalyptus and pinus on the deconstruction of the cell wall during the production of cellulose nanofibrils, Cellulose 28 (9) (2021) 5387–5399.
[56] J.B. Sluiter, R.O. Ruiz, C.J. Scarlata, A.D. Sluiter, D.W. Templeton, Compositional analysis of lignocellulosic feedstocks. 1. Review and description of methods, J. Agric. Food Chem. 58 (16) (2010) 9043–9053.
[57] J.L. Sanchez-Salvador, M.C. Monte, C. Negro, W. Batchelor, G. Garnier, A. Blanco, Simplification of gel point characterization of cellulose nano and microfibrils suspensions, Cellulose 28 (2021) 6995–7006.
[58] C. Campano, P. Lopez-Exposito, A. Blanco, C. Negro, T.G.M. van de Ven, Hairy cationic nanocrystalline cellulose as a novel flocculant of clay, J. Colloid Interface Sci. 545 (2019) 153–161.
[59] B. Nakao, C. Tanaka, A. Takahashi, Long-term changes in degree of crystallinity ofwood cellulose, Holzforschung 43 (6) (1989) 419–420.
[60] P. Ma, S. Fu, H. Zhai, K. Law, C. Daneault, Influence of TEMPO-mediated oxidation on the lignin of thermomechanical pulp, Bioresour. Technol. 118 (2012) 607–610.
[61] G.P. Ponzano, Sodium hypochlorite: history, properties, electrochemical production, in: Disinfection by Sodium Hypochlorite: Dialysis Applications, Karger Publishers, 2007, pp. 7–23.
[62] R. Motta Neves, K. Silveira Lopes, M.G. Zimmermann, M. Poletto, A.J. Zattera, Cellulose nanowhiskers extracted from TEMPO-oxidized curaua fibers, J. Nat. Fibers 17 (9) (2020) 1355–1365.
[63] M.-C. Hsieh, H. Koga, K. Suganuma, M. Nogi, Hazy transparent cellulose nanopaper, Sci. Rep. 7 (1) (2017) 1–7.
[64] F. Serra-Parareda, R. Aguado, Q. Tarrés, P. Mutjé, M. Delgado-Aguilar, Potentiometric back titration as a robust and simple method for specific surface area estimation of lignocellulosic fibers, Cellulose (2021) 1–11.
[65] M. Hall, P. Bansal, J.H. Lee, M.J. Realff, A.S. Bommarius, Cellulose crystallinity–a key predictor of the enzymatic hydrolysis rate, FEBS J. 277 (6) (2010) 1571–1582.
[66] S. Iwamoto, K. Abe, H. Yano, The effect of hemicelluloses on wood pulp nanofibrillation and nanofiber network characteristics, Biomacromolecules 9 (3) (2008) 1022–1026.
[67] S. Tanpichai, S.K. Biswas, S. Witayakran, H. Yano, Water hyacinth: a sustainable lignin-poor cellulose source for the production of cellulose nanofibers, ACS Sustain. Chem. Eng. 7 (23) (2019) 18884–18893.
[68] S. Matsuoka, H. Kawamoto, S. Saka, What is active cellulose in pyrolysis? An approach based on reactivity of cellulose reducing end, J. Anal. Appl. Pyrolysis 106 (2014) 138–146.
[69] L. Malucelli, M.D. Matos, C. Jordão, D. Lomonaco, L. Lacerda, M.D.S. Carvalho Filho, W. Magalhães, Influence of cellulose chemical pretreatment on energy consumption and viscosity of produced cellulose nanofibers (CNF) and mechanical properties of nanopaper, Cellulose 26 (3) (2019) 1667–1681.
[70] A. Björn, P.S. de La Monja, A. Karlsson, J. Ejlertsson, B.H. Svensson, Rheological characterization, Biogas 1 (2012) 63–76.
[71] D. Tatsumi, S. Ishioka, T. Matsumoto, Effect of fiber concentration and axial ratio on the rheological properties of cellulose fiber suspensions, Nihon Reoroji Gakkaishi 30 (1) (2002) 27–32.
[72] E. Lasseuguette, D. Roux, Y. Nishiyama, Rheological properties of microfibrillar suspension of TEMPO-oxidized pulp, Cellulose 15 (3) (2008) 425–433.
[73] D. Chen, T.G. van de Ven, Morphological changes of sterically stabilized nanocrystalline cellulose after periodate oxidation, Cellulose 23 (2) (2016) 1051–1059.
[74] Y. Zhou, T. Saito, L. Bergström, A. Isogai, Acid-free preparation of cellulose nanocrystals by TEMPO oxidation and subsequent cavitation, Biomacromolecules 19 (2) (2018) 633–639.
[75] M.-C. Li, Q. Wu, K. Song, S. Lee, Y. Qing, Y. Wu, Cellulose nanoparticles: structure–morphology–rheology relationships, ACS Sustain. Chem. Eng. 3 (5) (2015) 821–832.
[76] T. Turpeinen, A. Jäsberg, S. Haavisto, J. Liukkonen, J. Salmela, A.I. Koponen, Pipe rheology of microfibrillated cellulose suspensions, Cellulose 27 (1) (2020) 141–156.
[77] M. Rides, C. Allen, Slip Flow Measurement by Capillary Extrusion Rheometry, 2006.
[78] M.A. Hubbe, P. Tayeb, M. Joyce, P. Tyagi, M. Kehoe, K. Dimic-Misic, L. Pal, Rheology of nanocellulose-rich aqueous suspensions: a review, Bioresources 12 (4) (2017) 9556–9661.
[79] A.N. Nakagaito, H. Kondo, H. Takagi, Cellulose nanofiber aerogel production and applications, J. Reinf. Plast. Compos. 32 (20) (2013) 1547–1552.